Dalton Transactions

Ligand-Triplet Migration in Iridium(III) Cyclometalates Featuring ππ-Conjugated Isocyanide Ligands

Journal:	*Dalton Transactions*
Manuscript ID	DT-ART-06-2020-002100.R1
Article Type:	Paper
Date Submitted by the Author:	30-Jun-2020
Complete List of Authors:	Favale, Joseph; North Carolina State University, Department of Chemistry Hauke, Cory; North Carolina State University, Department of Chemistry Danilov, Evgeny; North Carolina State University, Department of Chemistry Yarnell, James; North Carolina State University, Department of Chemistry Castellano, Felix; North Carolina State University, Department of Chemistry

ARTICLE

Ligand-Triplet Migration in Iridium(III) Cyclometalates Featuring π-Conjugated Isocyanide Ligands†

Received 00th January 20xx,
Accepted 00th January 20xx

DOI: 10.1039/x0xx00000x

Joseph M. Favale Jr., Cory E. Hauke, Evgeny O. Danilov, James E. Yarnell, and Felix N. Castellano*

The manipulation of the triplet excited state manifold leads to large differences in the photophysical properties within a given class of metal-organic chromophores. By the appropriate choice of ancillary ligand, large changes can be made both to the order and nature of the lowest excited states and therefore to the resulting photophysical properties. Herein, a series of four *bis*-2-phenylpyridine (ppy) cyclometalated Ir(III) compounds bearing two arylisocyanide ligands were synthesized and photophysically characterized to understand the effects of using ancillary ligands featuring systematic changes in π-conjugation. By varying the arylisocyanide ligands, the photoluminescence quantum yield ranged from 5% to 49% and the excited state lifetime ranged between 24 μs and 2 ms. These variations in photophysical response are consistent with lowering the triplet ligand-centered (^{3}LC) state of the arylisocyanide ligand as the π system was extended, confirmed by 77 K photoluminescence emission spectra and ultrafast transient absorption experiments. The latter analysis gleaned detailed insight into the importance of the interplay of the ^{3}LC state of the phenylpyridine and arylisocyanide ligands in these polychromophic Ir(III) molecules.

Introduction

Chromophore design directly impacts photophysical properties and there are a number of control elements that can be leveraged. For a molecule to display useful characteristics such as high photoluminescence (PL) quantum yield, a high level of photostability, and a long lifetime, the nature of the excited state manifold(s) must be considered. Metal-to-ligand charge transfer (MLCT) and ligand-centered (LC) π-π* states possess unique and characteristic non-radiative pathways for relaxing the chromophore to the ground state, in addition to distinctive radiative rate constants. Therefore, the ordering and energetic spacing within the excited state manifold profoundly affects the overall photophysical properties of the chromophore and the resultant properties can be envisioned as a superposition of the contributing excited states.

Cyclometalated Ir(III) transition metal complexes take advantage of excited state mixing to combine the benefits of ^{3}MLCT and ^{3}LC excited states that are sufficiently close in energy.[1, 2] This mixing results in a class of chromophores with highly desirable photophysical properties[3-6] suitable for a variety of optical applications including luminescence-based sensing,[7-9] light-emitting devices,[10-12] and imaging.[13-15] Heteroleptic cyclometalated Ir(III) molecules of the formula $[Ir(C^N)_2LL']^{0/+}$, where (C^N) is the cyclometalating ligand such as 2-phenylpyridine (ppy) and L and L' are the ancillary ligand(s), are among the more popular structural motifs.[16] Modifying either the cyclometalating ligand or the ancillary ligand deliberately manipulates the excited state energetics, thereby altering the photophysical properties of the molecule.[17]

Isocyanide-based ancillary ligands have profound effects on the photophysical properties of transition metal complexes.[18-22] The strong σ-donating character of these ligands elevates the energy of the σ-antibonding d-orbitals of the metal center; the pseudo e_g orbitals for pseudo-octahedral complexes. At the same time, the propensity of the isocyanide subunit to engage in π-backbonding necessarily increases the energy of the associated MLCT excited state.[23-25] Previous studies by Thompson and coworkers[26] and Nazeeruddin, along with Shavaleev and Armaroli[27-29] and Fantacci[30] produced Ir(III) *bis*-cyclometalated complexes bearing either one or two alkyl isocyanides. These molecules display highly photoluminescent excited states which have been assigned to the triplet ligand-centered (^{3}LC) state of the cyclometalating ligand, as the MLCT excited state shifts to higher energies as a result of the conspiring ligand electronic effects. Teets and co-workers expanded the scope of this motif with the incorporation of 2,6-diisopropylphenyl, 2,6-dimethylphenyl, and 2-naphthyl isocyanides.[21, 22, 31] The lowest triplet state of these molecules again had a high level of ^{3}LC character from the cyclometalating ligand. Critically, the use of aryl isocyanides offers the synthetically accessible 4-position of the aromatic ring enabling facile synthetic modification of the ligand.

A second strategy to combine the benefits of a higher energy ^{3}MLCT and a lower energy ^{3}LC state is to engineer thermal equilibrium by maintaining a small energy gap between these two states.[18, 32-37] The molecule then will have the PL spectral and quantum yield properties of the MLCT excited state

* Department of Chemistry, North Carolina State University, Raleigh, NC 27695-8204, USA. E-mail: fncastel@ncsu.edu

†Electronic Supplementary Information (ESI) available: NMR and FTIR spectra, nanosecond transient absorption data, ultrafast transient absorption and computational analyses. See DOI: 10.1039/x0xx00000x

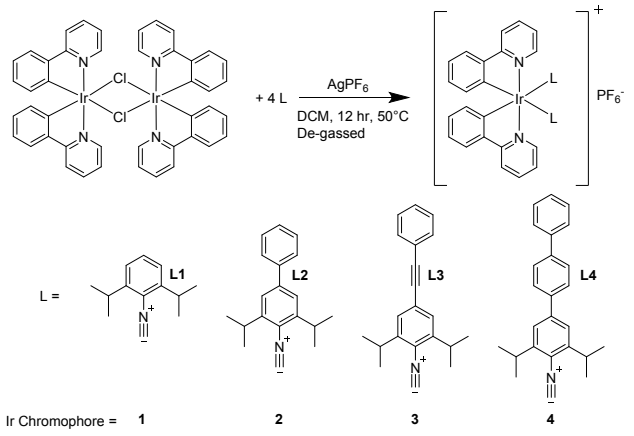

Scheme 1 Generalized reaction used for the formation of molecules **1-4** in this study.

while possessing a significantly extended excited state lifetime; the latter results from thermal activation by the ^{3}LC excited state. Demas and DeGraff[18] and Rillema[38] synthesized Re(I) phenanthroline tricarbonyl chromophores with such equilibria that extended the excited state lifetime of these molecules from tens to hundreds of microseconds. Another common method for introducing this equilibrium into the triplet manifold is to append selected organic chromophore(s) with the appropriate triplet energetics to interact with the charge transfer state. For example, we have demonstrated the benefits of this approach in Ru(II) polypyridyl,[33, 34] Re(I) tricarbonyl, [35, 39] and Pt(II) dimer chromophores.[40]

In the present contribution, a series of Ir(III) *bis*-cyclometalated chromophores, presented in Scheme 1, have been designed to leverage both excited state mixing and thermal equilibria. By systematically increasing the conjugation of the aryl isocyanide ancillary ligands, the energy of its ^{3}LC manifold was tuned from being the highest energy state (**1**), to being in equilibrium with the ^{3}LC (ppy) state (**2**), to being the lowest energy excited state (**3** and **4**). The ordering of these states markedly impacted the observed photophysical properties including the PL emission energy, quantum yield, and excited state lifetime. Ultrafast transient absorption experiments and electronic structure calculations provided detailed insight into the interactions of the three triplet excited states in these manifolds.

Experimental

General Procedures. All reagents and solvents used in the synthetic procedures were obtained from commercial sources and used as received, unless otherwise noted. The isocyanide ligands used for each complex were obtained using previously published syntheses.[39] ^{1}H and ^{13}C NMR spectra were recorded on a Varian Innova 400 MHz spectrometer with working frequencies of 400 and 100 MHz for ^{1}H and ^{13}C NMR, respectively. All NMR spectra were plotted and processed using MestReNova software, version 10.0.2. High-resolution ESI-MS data were measured at the Michigan State University Mass Spectrometry and Metabolomics Core (Waters Xevo G2-XS QTOF). Electronic absorption spectroscopic measurements were recorded on a Shimadzu UV-3600 spectrophotometer in 1 cm quartz cuvettes with spectrophotometric-grade THF as the solvent. Steady-state emission measurements were made on an FS-980 fluorimeter (Edinburgh Instruments) fitted with a 450 W xenon arc lamp and a PMT detector in a sealable 1 cm quartz cuvette designed for air-free handling. Quantum yields were measured relative to 9,10-diphenylanthracene in cyclohexane for **1** and **2**, and quinine sulfate in 0.5 M H_2SO_4 for **3** and **4**, ±10%.[41]

Synthesis of [(μ-Cl)Ir(ppy)$_2$]$_2$. The synthesis was performed based on a previously published procedure.[3] In a 250 mL, 2-neck round-bottom flask fitted with a reflux condenser, Ir(III)trichloride hydrate (846 mg, 2.67 mmol) and 2-phenylpyridine (ppy, 869 mmol, 5.59 mmol) were dissolved in 100 mL of 2-ethoxyethanol:deionized water (3:1 v/v). This solution was bubble degassed with N_2 for 20 min then heated to 115°C for 3 hr under N_2 atmosphere. The reaction was then allowed to cool to room temperature, then further cooled to 0°C to induce precipitation of the product. The yellow precipitated product was filtered and washed with absolute ethanol and acetone and dried in vacuo. Yield: 985 mg, 76.5%. ^{1}H NMR (400 MHz, CD_2Cl_2): δ 9.25 (d, 4H, *J* = 5.8 Hz), 7.93 (d, 4H, *J* = 8.2 Hz), 7.80 (t, 4H, *J* = 8.2 Hz), 7.55 (d, 4H, *J* = 7.8 Hz), 6.81 (m, 8H), 6.60 (t, 4H, *J* = 7.8 Hz), 5.87 (d, 4H, *J* = 7.8 Hz).

General Procedure for Synthesis of Ir-CNAr Complexes (Scheme 1). In a 50 mL, 2-neck round-bottom flask fitted with a reflux condenser, [(μ-Cl)Ir(ppy)$_2$]$_2$, CNAr ligand (4 eq.) and $AgPF_6$ (5 eq.) were degassed via three cycles of vacuum-N_2 backfill and then maintained under N_2 atmosphere. To these solids, 25 mL of N_2 bubble degassed dichloromethane was added. The reaction mixture was protected from light and heated to 50°C for 12 h. The reaction was then filtered hot over Celite and the filtrate was evaporated. The crude product was dissolved in minimal methanol and a solution of sat. aqueous NH_4PF_6 was added dropwise to precipitate the product. The solids were filtered and rinsed with excess deionized water and dried *in vacuo*. This methanol/NH_4PF_6 recrystallization procedure was repeated twice to ensure product purity.

[*cis*-Ir(ppy)$_2$(DippCN)$_2$]PF$_6$ (1). [(μ-Cl)Ir(ppy)$_2$]$_2$ (100 mg, 0.093 mmol), 2,6-diisopropylphenyl isocyanide (**L1**, 70 mg, 0.373 mmol), and $AgPF_6$ (117 mg, 0.463 mmol) were used. Yield: 156 mg, 82%. ^{1}H NMR (400 MHz, CD_2Cl_2): δ 9.14 (d, 2H, *J* = 6.2 Hz), 8.11 (m, 4 H), 7.78 (d, 2H, *J* = 8.3 Hz), 7.37 (m, 4H), 7.17 (d, 4H, *J* = 7.8 Hz), 7.13 (t, 2H, *J* = 7.5 Hz), 7.02 (t, 2H, 7.5 Hz), 6.31 (d, 2H, *J* = 7.5 Hz), 2.79 (sep, 4H, *J* = 6.7 Hz), 1.05 (m, 24H). ^{13}C NMR (100 MHz, CD_2Cl_2): δ 168.3, 153.8, 152.7, 146.1, 144.5, 140.0, 137.0, 131.7, 131.4, 131.1, 125.7, 125.1, 124.8, 124.3, 124.2, 121.7, 30.7, 22.8, 22.7. HR-MS ([M-PF$_6$]$^+$). Calcd: *m/z* 873.3641. Found: *m/z* 873.3638. FTIR (ATR, cm^{-1}): 2170 (sh), 2143 (s).

[*cis*-Ir(ppy)$_2$(PhDippCN)$_2$]PF$_6$ (2). [(μ-Cl)Ir(ppy)$_2$]$_2$ (100 mg, 0.093 mmol), 4-phenyl-2,6-diisopropylphenyl isocyanide (**L2**, 100 mg, 0.380 mmol), and $AgPF_6$ (117 mg, 0.463 mmol) were used. Yield: 168 mg, 77%. ^{1}H NMR (400 MHz, CD_2Cl_2): δ 9.17 (d, 2H, *J* = 5.5 Hz), 8.11 (m, 4 H), 7.80 (d, 2H, *J* = 7.9 Hz), 7.55 (m,

4H), 7.45–7.38 (d, 12H), 7.15 (t, 2H, *J* = 7.5 Hz), 7.04 (t, 2H, 7.5 Hz), 6.33 (d, 2H, *J* = 7.5 Hz), 2.87 (sep, 4H, *J* = 6.9 Hz), 1.12 (m, 24H). ^{13}C NMR (100 MHz, CD_2Cl_2): δ 168.4, 153.8, 152.7, 146.5, 144.5, 144.3, 140.3, 140.0, 131.8, 131.2, 129.5, 129.0, 127.7, 125.8, 125.7, 125.1, 124.9, 123.1, 121.7, 121.6, 30.8, 22.9, 22.8. HR-MS ($[M\text{-}PF_6]^+$). Calcd: *m/z* 1025.4267. Found: *m/z* 1025.4247. FTIR (ATR, cm^{-1}): 2168 (sh), 2143 (s).

[*cis*-Ir(ppy)$_2$(PhEthDippCN)$_2$]PF$_6$ (3). [(μ-Cl)Ir(ppy)$_2$]$_2$ (100 mg, 0.093 mmol), 4-phenylethynyl-2,6-diisopropylphenyl isocyanide (**L3**, 108 mg, 0.376 mmol), and $AgPF_6$ (117 mg, 0.463 mmol) were used. Yield: 163 mg, 72%. ^{1}H NMR (400 MHz, CD_2Cl_2): δ 9.13 (d, 2H, *J* = 5.9 Hz), 8.12 (m, 4 H), 7.80 (d, 2H, *J* = 7.7 Hz), 7.53 (m, 4H), 7.38 (m, 8H), 7.33 (s. 4H), 7.14 (t, 2H, *J* = 7.4 Hz), 7.03 (t, 2H, 7.4 Hz), 6.30 (d, 2H, *J* = 7.6 Hz), 2.79 (sep, 4H, *J* = 6.8 Hz), 1.08 (m, 24H). ^{13}C NMR (100 MHz, CD_2Cl_2): δ 168.3, 153.8, 152.5, 146.3, 144.5, 140.1, 138.1, 132.2, 131.8, 131.1, 129.6, 129.1, 127.5, 126.4, 125.7, 125.1, 125.0, 123.8, 122.9, 121.8, 92.7, 88.7, 30.6, 22.7, 22.6. HR-MS ($[M\text{-}PF_6]^+$). Calcd: *m/z* 1073.4267. Found: *m/z* 1073.4259. FTIR (ATR, cm^{-1}): 2166 (sh), 2140 (s).

[*cis*-Ir(ppy)$_2$(DiPhDippCN)$_2$]PF$_6$ (4). [(μ-Cl)Ir(ppy)$_2$]$_2$ (100 mg, 0.093 mmol), 4-biphenyl-2,6-diisopropylphenyl isocyanide (**L4**, 130 mg, 0.383 mmol), and $AgPF_6$ (117 mg, 0.463 mmol) were used. Yield: 182 mg, 74%. ^{1}H NMR (400 MHz, CD_2Cl_2): δ 9.19 (d, 2H, *J* = 5.8 Hz), 8.13 (m, 4 H), 7.81 (d, 2H, *J* = 7.8 Hz), 7.70 (m, 4H), 7.65 (m, 8H), 7.49-7.36 (m. 12H), 7.16 (t, 2H, *J* = 7.4 Hz), 7.05 (t, 2H, 7.4 Hz), 6.34 (d, 2H, *J* = 7.5 Hz), 2.89 (sep, 4H, *J* = 6.9 Hz), 1.14 (m, 24H). ^{13}C NMR (100 MHz, CD_2Cl_2): δ 168.4, 153.8, 152.7, 146.6, 144.5, 143.7, 141.7, 140.6, 140.0, 139.1 137.6, 131.7, 131.2, 129.5, 128.3, 128.1 (2C), 127.5, 125.7, 125.1, 124.9, 123.3, 123.0, 121.7, 30.8, 22.9, 22.8. HR-MS ($[M\text{-}PF_6]^+$). Calcd: *m/z* 1177.4893. Found: *m/z* 1177.4897. FTIR (ATR, cm^{-1}): 2168 (sh), 2141 (s).

Ultrafast Transient Absorbance (TA) Spectroscopy. Time-resolved TA measurements were performed at the North Carolina State University Imaging and Kinetic Spectroscopy Laboratory in the Department of Chemistry. Sub-picosecond absorption transients were detected using a Helios transient absorption spectrometer from Ultrafast Systems. A portion of the output from a 1 kHz Ti:Sapphire Coherent Libra regenerative amplifier (4 mJ; 100 fs fwhm at 800 nm) was split into the pump and probe beams. The probe beam was delayed in a 6 ns optical delay stage, while the pump beam was directed into an optical parametric amplifier (Coherent OPerA Solo) to generate tunable excitation. These measurements and data analyses were performed according to previously published methods.[35, 42]

Nanosecond TA Spectroscopy. Nanosecond TA measurements were collected with a LP920 laser flash photolysis system (Edinburgh Instruments) using a Minilite 355 Nd:YAG (Continuum) as the excitation source. TA difference spectra were collected using an iStar ICCD camera (Andor Technology), controlled by the LP900 software (Edinburgh Instruments).

Density Functional Theory (DFT) Calculations. The calculations utilized in this study were performed using the Gaussian 09 software package (revision D.01)[43] and the computation resources of the North Carolina State University High Performance Computing Center. Ground state and triplet state geometry optimizations were performed using the M06 functional,[44] along with the def2-SVP basis set of the Alrichs group as implemented in Gaussian 09.[45] The Stuttgart–Dresden effective core potentials (ECPs)[46] were used to replace the core electrons in iridium for all calculations. The polarizable continuum model (PCM) was used to simulate the tetrahydrofuran solvent environment for all calculations.[47] Frequency calculations were performed on all optimized structures and no imaginary frequencies were obtained. The time dependent (TD)-DFT calculations were performed using the same conditions as described for the geometry optimizations.[48-50] The energy and oscillator strengths were computed for each of the 50 lowest singlet excitations and 10 lowest triplet excitations. The natural transition orbitals of the low-lying singlet and triplet transitions were generated using GaussView 5.0.[51]

Results and Discussion

Electronic Structure Calculations

DFT calculations were performed on **1**-**4** to support the excited state assignments observed in this study. The M06 functional and the Def2-SVP basis set were used in our previous Re(I) aryl-isocyanide study and were used here as a starting point.[39] Benchmarking was performed using multiple hybrid functionals against the crystal structure[22] of the dimethylphenylisocyanide analog of **1** (**Table S1**). In general, the three functionals benchmarked performed similarly when evaluating bond lengths and bond angles around the iridium atom. The M06 functional performed slightly better when evaluating the molecular overlay between the optimized structure and the crystal structure, with much of the difference arising from the rotation of the aryl ring on the isocyanide ligand (**Figure S21**).

The geometries of **1**-**4** were optimized at the PCM/M06/Def2-SVP/SDD level of theory, with the results presented in **Table S2**. When comparing the structure of **1** to the dimethylphenylisocyanide analog, the incorporation of the isopropyl groups on the phenyl rings does not change the bonding environment around the iridium atom significantly, with comparable bond lengths and bond angles. The extension of the isocyanide ligand results in the angle between the two isocyanide ligands coming closer to 90°, likely from London dispersion forces counteracting the steric repulsion of the isopropyl groups. In addition, the isocyanide becomes more linear (approaching 180°) as the conjugation length of the ligands is increased.

The calculated frontier molecular orbital diagrams of **1**-**4** are presented in **Figures S23-S26** with a simplified view presented in **Figure 1**. For **1**, the HOMO − 1 and HOMO are the out-of-phase and in-phase **π**-bonding orbitals, respectively, that are localized on the ppy ligand with a small contribution of the iridium in the HOMO. Similarly, the LUMO and LUMO + 1 are the out-of-phase and in-phase **π**-antibonding orbitals, respectively, that are also localized on the ppy ligand. When an additional phenyl ring is added to the isocyanide ligand as in **2**, the HOMO becomes partially localized on both the isocyanide and the ppy ligands, with some contribution from the

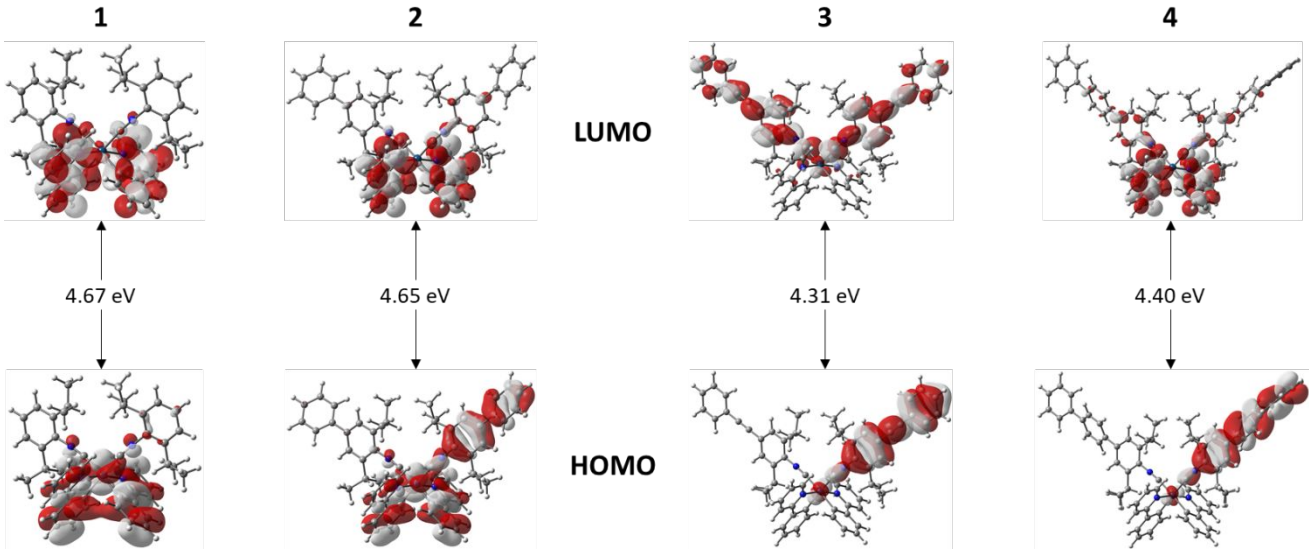

Fig. 1 Simplified frontier orbital diagrams constructed for **1**-**4**. Calculations performed at DFT//PCM/M06/Def2-SVP/SDD level of theory.

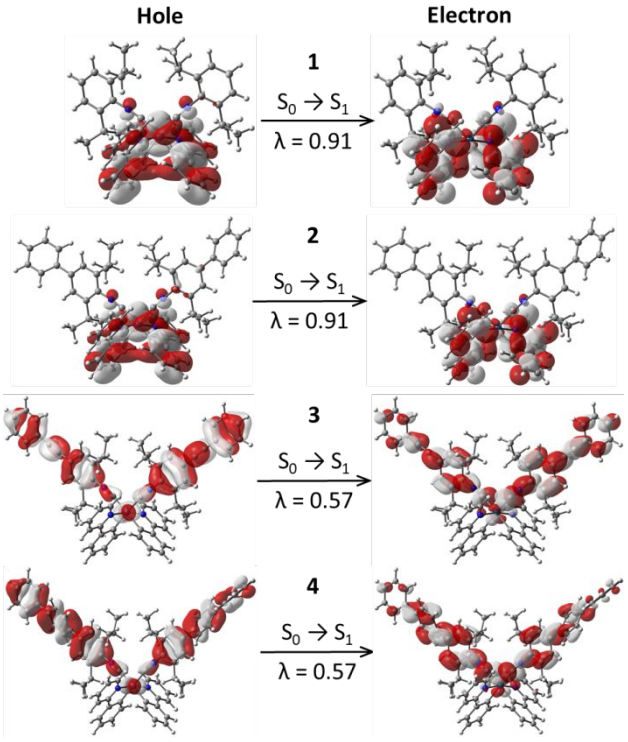

Fig. 2 Natural transition orbitals (NTOs) for $S_0 \rightarrow S_1$ excitations of **1**-**4** determined at the TD-DFT//PCM/M06/Def2-SVP/SDD level of theory. λ is the fraction of the hole–particle contribution to the excitation.

metal center. The HOMO − 1 is almost exclusively localized on the isocyanide ligand. The LUMO and LUMO + 1 are still localized on the ppy ligand and are similar in composition and energies to those observed in **1**. In **3**, the addition of the phenyl acetylene subunit to the isocyanide ligand results in the HOMO − 1, HOMO, LUMO, and LUMO + 1 being localized primarily on the isocyanide ligand, with a small contribution from the metal atom. When substituting to three phenyl rings in **4**, the HOMO and HOMO − 1 remaining largely unchanged, where the LUMO and LUMO + 1 localize mainly on the ppy ligands, with a small component on the isocyanide ligand. Across the series, the HOMO-LUMO gap reduces from 4.67 eV (**1**) to 4.31 eV (**3**) as the conjugation across the isocyanide ligand increases. Despite the additional aryl ring in **4**, the HOMO-LUMO gap increases to 4.40 eV, likely arising from the twisted nature of the three adjacent phenyl rings.

Static Absorption and PL Measurements

The electronic absorption and steady-state PL spectra of **1**-**4** are presented in **Figure 3**. The lowest energy bands for all complexes occur at 350 nm. The assignment of the band at 350 nm in all molecules can be made as metal-to-ligand and intraligand charge transfer (MLCT and ILCT, respectively), specifically from the Ir d-orbitals and phenyl π-orbitals to the pyridyl π*-orbitals. A pair of higher energy bands red shift across the series, and these are assigned to the π → π* transitions of the isocyanide ligands. These bands shift from 258 and 288 nm in **1** to a single strong band at 312 nm in **4.** In addition to this bathochromic shift, the molar extinction coefficients of these bands increase across the series, providing evidence of the extended π-conjugation of **L4** as compared to **L1**. The intense π → π* electronic transitions are also supported by the TD-DFT calculations which manifest as $S_0 \rightarrow S_1$ and $S_0 \rightarrow S_3$ in **1** and **2**, respectively, to $S_0 \rightarrow S_1$ in **3** and **4** (**Figure 2**). The TD-DFT calculations do underestimate the energy of this transition, however, the trend from **1** to **4** is conserved across the series.

The photoluminescence spectrum of **1** was previously reported by Teets and coworkers.[22] They assigned the PL emission as having significant ppy character. The structure and energy of the PL of **2** is nearly identical to that of **1**, suggesting identical excited state character. The radiative rate constant (k_r) for **2** is less than half that of **1**, suggesting either more ligand-centered character or an equilibrium with a longer-lived triplet excited state. The PL emission of **3** and **4** are red-shifted from

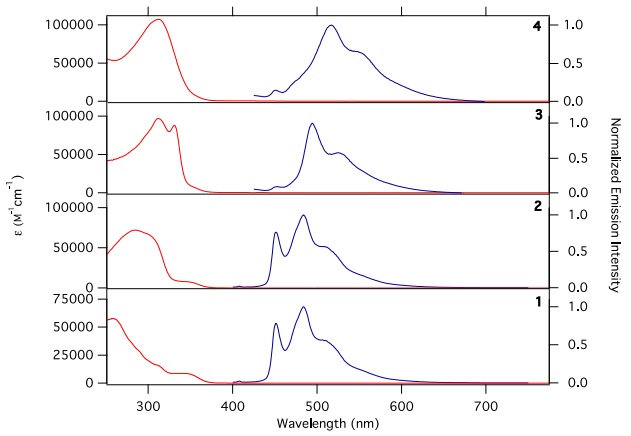

Fig. 3 Electronic UV-vis absorbance (red) and normalized static PL (blue) spectra (λ_{ex} = 355 nm) of **1–4** measured in THF at RT. The PL spectra were recorded with samples having an O.D. = 0.1 at 355 nm in deoxygenated THF.

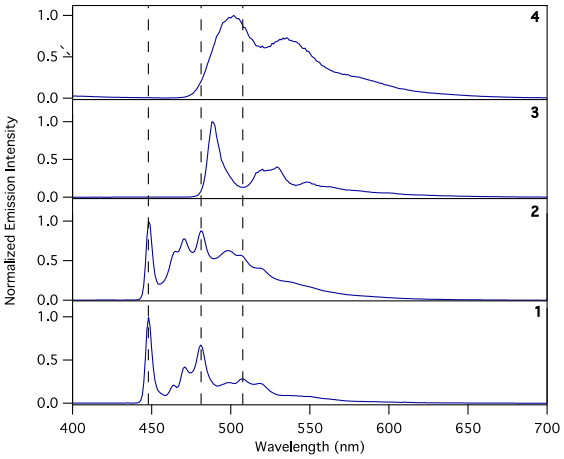

Fig. 4 Normalized static PL spectra of **1–4** measured in 2-MeTHF frozen glasses at 77 K (λ_{ex} = 355 nm). The vertical dashed lines are drawn as a guide for the eye to illustrate the marked differences in the PL spectral profiles in **1** and **2** with respect to **3** and **4**.

that of **1** and **2**, have a lower quantum yield, and significantly lower radiative rate constants (k_r). The k_r values of **3** and **4** are much smaller and the lifetimes are longer than what would be expected from a pure MLCT excited state. These bands are assigned to the $\pi^* \rightarrow \pi$ of the isocyanide ligands **L3** and **L4**.

Static PL measurements were performed in a frozen matrix of 2-methyltetrahydrofuran (2-MeTHF) at 77 K and are presented in **Figure 4**. Molecules **1** and **2** again behave congruently. There are slight differences in the shape of the emission spectra at 77 K that suggest some contribution from **L2** might be present. This interpretation is supported by the triplet TD-DFT calculations that predict the triplet states of the ppy and the **L2** ligand should be nearly isoenergetic (see **Table S4** and **Figure S28**). Mixing of the ppy and isocyanide ligand-centered states would also explain the decrease in radiative rate constant observed in **2** as compared to **1**. The thermally-induced shift [ΔE_S = E_{00}(77K) – E_{00}(298K)], which qualitatively reports the degree of CT character present in the excited state, is 148 cm^{-1} in both molecules. This value points to little to no CT contribution to the emissive excited state. Molecules **3** and **4** possess quantitatively similar 77 K emission spectra with respect to each other, but are notably different in both shape and energy from that measured in **1** and **2**. This is a clear indication that the lowest energy excited state is distinct and is assigned as residing on the isocyanide ligand. This is also consistent with the assignment of the RT PL emission spectra of **3** and **4** described earlier.

Excited-State Dynamics

The ultrafast TA difference spectra of each chromophore is presented in **Figure 5**, with the time constants fit to the most prominent transient signals summarized in **Table 2**. In **1**, the initially formed transient represents the formation of a mixed state of mostly ^{3}LC (ppy) character, with a small degree of Ir(III) d-character. As seen in numerous related examples, the transient signal observed is dominated by that of the ^{3}LC excited state.[33-36, 40, 52-54] The ^{3}LC state on ppy forms in pulse (sub-ps), representative of the rapid intersystem crossing (ISC) rate from the singlet manifold. Once formed, there are 5.5 and 79 ps time constants that are associated with internal conversion processes within the ppy triplet manifold. The difficulty in definitive assignment of these time constants is due to the convoluted spectral shifts observed on these time scales.

In **2** and **3**, significantly different dynamics are observed. The initially formed excited state is similar to the prompt signal observed in **1**, suggesting that the initial ISC pathway to the ^{3}LC (ppy) state is preserved. Similar to **1**, both complexes possess a

Table 1. Summary of photophysical parameters of **1–4**.

Complex	Abs λ_{max}, nm (ε, $M^{-1}cm^{-1}$)[a]	RT PL λ_{max}, nm[a]	77 K PL λ_{max}, nm[a]	ΔE_S, cm^{-1}	Φ	τ_{TA}, μs	k_r, s^{-1} [c]	k_{nr}, s^{-1} [c]
1	258 (57700), 311 (16100), 346 (sh) (8500)	451, 484, 514	448, 481, 507	148	0.49	24	20000	21000
2	286 (72000), 308 (59600), 346 (sh) (7900)	451, 484, 514	448, 481, 507	148	0.49	61	8000	8300
3	312 (97000), 331 (88000), 352 (sh) (8300)	494, 526	488, 529. 548	249	0.050	370[b]	130	2500
4	312 (107400)	517, 554	502, 535, 581	578	0.070	2000[b]	40	500

[a] All RT spectra measured in THF (absorption), deoxygenated THF (PL), and 77 K PL data recorded in Me-THF frozen glass. All wavelengths measured to ±2 nm.
[b] Excited-state lifetime extrapolated to infinite dilution, ±5%, see Ref 39.
[c] $k_r = \Phi/\tau$, $k_{nr} = (1-\Phi)/\tau$

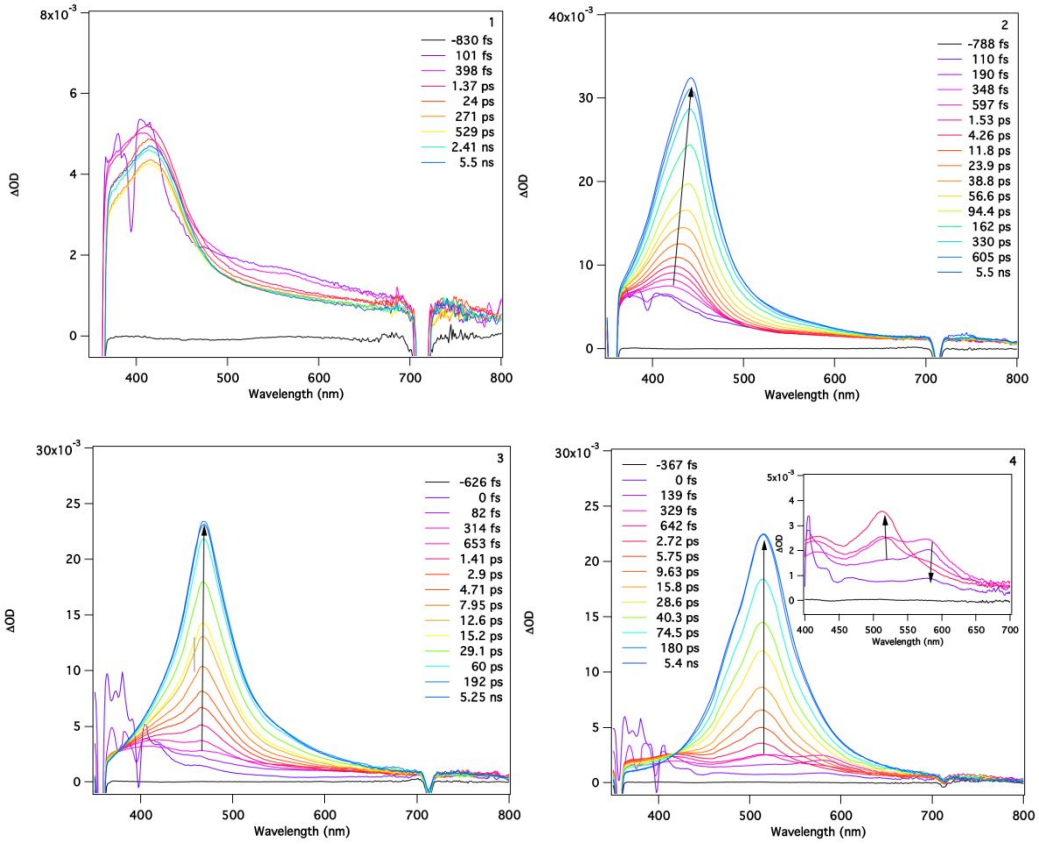

Fig. 5 Ultrafast TA difference spectra of **1–4** recorded in THF. The inset of **4** displays the prompt transients (<2.72 ps) in closer detail. All difference spectra were obtained using 356 nm excitation (0.3 μJ/pulse for **1** and **2**, 0.2 μJ/pulse for **3** and **4**; 100 fs fwhm) with sample O.D.'s of ~0.45.

short time constant, in this case 2 ps, which again is assigned to triplet internal conversion. Afterwards, a new signal grows in with a time constant of 130 ps and 22 ps in **2** and **3** respectively. This signal then persists for the remainder of the ultrafast experiment. This strongly absorbing transient is assigned, based on previous isocyanide complexes and free ligand triplet sensitization,[39] as the pure ^{3}LC of the isocyanide fragment. The time constants associated with the growth of these signals represent triplet migration between these spatially separate ligands. The triplet manifolds in **2** are sufficiently isoenergetic that at room temperature, thermal equilibrium can be established between these states. This observation is supported by the triplet TD-DFT calculations as the lowest three transitions are nearly isoenergetic with the ^{3}LC (**L2**) states ($S_0 \rightarrow T_1$ and $S_0 \rightarrow T_2$) being lowest in energy and the ^{3}LC (ppy) state ($S_0 \rightarrow T_3$) being slightly higher (**Table S4** and **Figure S28**). This explains the longer lifetime of **2** compared to **1**, despite emission envelopes of similar energy and shape. The faster time constant for the population of ^{3}LC (**L3** state in **3** as compared to **2**, when taken in context with the photoluminescence data, shows a more complete depopulation of the ^{3}LC (ppy) state.

There are differences in the early-timepoint TA spectra of **4** compared to the other complexes. In addition to the initial band at 410 nm that is the signature of the ^{3}LC (ppy) state, a second band at 570 nm appears within the pulse. This band decays away, or is subsumed by the growing band at 515 nm, after 3 ps. The assignment of this band would be consistent with a charge transfer band involving the now lower-lying π* orbitals of **L4**. This is a higher energy triplet state than either the ^{3}LC (**L4**) or the ^{3}LC (ppy), thus explaining its rapid depopulation.

In all four complexes, the transient signal at the longest delay time persists into the nanosecond TA experiment. The lifetimes of the nanosecond transients are given in **Table 1**. The magnitude (tens to hundreds of μs) is consistent with the lowest triplet assignments being predominantly ^{3}LC (ppy for **1** and **2** or isocyanide for **3** and **4**) in character. The nanosecond TA difference spectra, as well as relevant kinetic data are provided in the SI, **Figure S10** and **S11**.

Table 2. Summary of the time constants from ultrafast TA kinetic modeling of **1–4**.[a]

Complex	λ_{fit} (nm)	τ_1 (ps)	τ_2 (ps)
1	380, 410, 456, 570	5.5	79
2	388, 412, 442, 517	2	130
3	472	2	22
	377	0.3	--
4	514	8	46
	571	0.3	0.3

[a] - Fits and kinetic data from which these time constants were obtained can be found in **Figures S12** through **S20**

Conclusions

A series of Ir(III) *bis*-ppy cyclometalated complexes featuring arylisocyanide ancillary ligands with varying amounts of π-conjugation were synthesized. The experimental evidence suggests that the degree of π-conjugation appended to the isocyanide ligand, which lowers the isocyanide ligand's triplet

energy, imparts significant changes to the excited state dynamics and to the lowest energy excited state in the manifold. In **1**, the lowest triplet state is predominantly ^{3}LC (ppy) in character. The emission of **2** is the same as that of **1**, suggesting the same ^{3}LC (ppy) emitting state, however the lifetime is longer by a factor of three which suggests an equilibrium with another, longer lived, ligand-centered state. The existence of this state is confirmed by ultrafast TA where a band assigned to the ^{3}LC (isocyanide) ligand grows in with a time constant of 130 ps. The combined experiments suggest an equilibrium between the ^{3}LC (ppy) and the ^{3}LC (isocyanide) in **2**. By contrast, the emission of **3** is at a lower energy and of a different shape than **1** and **2**, along with having a lifetime greater by an order of magnitude. Additionally, the strong band at 472 nm in the ultrafast TA grows in much faster than in **2** with a time constant of 22 ps. The data here is consistent with emission now coming from the ^{3}LC (isocyanide) state. Finally, in **4**, a similar picture emerges with the addition of what is most likely a short-lived higher energy charge transfer state likely from the iridium to the isocyanide ligand. The findings across the series are consistent with the extension of conjugation of the arylisocyanide's π system and thus the lowering in energy of that state as the series progresses. This series of iridium complexes demonstrate how by ligand design, the triplet excited state manifold can be manipulated to change the resultant photophysical properties of the iridium chromophore.

Conflicts of interest

There are no conflicts to declare.

Acknowledgements

This work was supported by the U.S. Department of Energy, Office of Science, Office of Basic Energy Sciences, under Award DE-SC0011979. J.E.Y. was supported by the Air Force Institute of Technology (AFIT).

References

1. M. G. Colombo, A. Hauser and H. U. Guedel, *Inorg. Chem.*, 1993, **32**, 3088-3092.
2. M. G. Colombo and H. U. Guedel, *Inorg. Chem.*, 1993, **32**, 3081-3087.
3. S. Sprouse, K. A. King, P. J. Spellane and R. J. Watts, *J. Am. Chem. Soc.*, 1984, **106**, 6647-6653.
4. K. A. King, P. J. Spellane and R. J. Watts, *J. Am. Chem. Soc.*, 1985, **107**, 1431-1432.
5. T. Sajoto, P. I. Djurovich, A. B. Tamayo, J. Oxgaard, W. A. Goddard and M. E. Thompson, *J. Am. Chem. Soc.*, 2009, **131**, 9813-9822.
6. J. C. Deaton and F. N. Castellano, in *Iridium(III) in Optoelectronic and Photonics Applications*, ed. E. Zysman-Colman, John Wiley and Sons Inc., Chichester, West Sussex, 1 edn., 2017, ch. 1, pp. 1-69.
7. K. Y. Zhang, P. Gao, G. Sun, T. Zhang, X. Li, S. Liu and Q. Zhao, *J. Am. Chem. Soc.*, 2018, **140**, 7827-7834.
8. Z. Du, R. Zhang, B. Song, W. Zhang, Y.-L. Wang, J. Liu, C. Liu, Z. P. Xu and J. Yuan, *Chem. Eur. J.*, 2019, **25**, 1498-1506.
9. K. Ohno, T. Sakata, M. Shiiba, A. Nagasawa and T. Fujihara, *Dalton Trans.*, 2019, **48**, 8068-8075.
10. N. Su, Z.-G. Wu and Y.-W. Zheng, *Dalton Trans.*, 2018, **47**, 7587-7593.
11. H.-H. Kuo, Y.-T. Chen, L. R. Devereux, C.-C. Wu, M. A. Fox, C.-Y. Kuei, Y. Chi and G.-H. Lee, *Adv. Mater.*, 2017, **29**, 1702464.
12. X. Yang, G. Zhou and W.-Y. Wong, *Chem. Soc. Rev.*, 2015, **44**, 8484-8575.
13. K. Y. Zhang, T. Zhang, H. Wei, Q. Wu, S. Liu, W. Zhao and W. Huang, *Chem. Sci.*, 2018, **9**, 7236-7240.
14. F. Schibilla, A. Holthenrich, B. Song, A. L. L. Matos, D. Grill, D. R. Martir, V. Gerke, E. Zysman-Colman and B. J. Ravoo, *Chem. Sci.*, 2018, **9**, 7822-7828.
15. G. Zhang, H. Zhang, Y. Gao, R. Tao, L. Xin, J. Yi, F. Li, W. Liu and J. Qiao, *Organometallics*, 2014, **33**, 61-68.
16. C. K. Prier, D. A. Rankic and D. W. C. MacMillan, *Chem. Rev.*, 2013, **113**, 5322-5363.
17. A. F. Henwood and E. Zysman-Colman, *Chem. Commun.*, 2017, **53**, 807-826.
18. L. Sacksteder, M. Lee, J. N. Demas and B. A. DeGraff, *Journal of the American Chemical Society*, 1993, **115**, 8230-8238.
19. J. M. Villegas, S. R. Stoyanov, W. Huang and D. P. Rillema, *Inorganic Chemistry*, 2005, **44**, 2297-2309.
20. C.-C. Ko, A. W.-Y. Cheung, L. T.-L. Lo, J. W.-K. Siu, C.-O. Ng and S.-M. Yiu, *Coord. Chem. Rev.*, 2012, **256**, 1546-1555.
21. H. Na, A. Maity and T. S. Teets, *Dalton Trans.*, 2017, **46**, 5008-5016.
22. A. Maity, Q. L. Le, Z. Zhu, J. Bao and T. S. Teets, *Inorg. Chem.*, 2016, **55**, 2299-2308.
23. Y. Yamamoto, *Coord. Chem. Rev.*, 1980, **32**, 193-233.
24. R. H. Crabtree, *The Organometallic Chemistry of the Transition Metals*, John Wiley & Sons, New Jersey, 4th edn., 2005.
25. J. F. Hartwig, *Organotransition Metal Chemistry. From Bonding to Catalysis.*, University Science Books, 1st edn., 2010.
26. J. Li, P. I. Djurovich, B. D. Alleyne, M. Yousufuddin, N. N. Ho, J. C. Thomas, J. C. Peters, R. Bau and M. E. Thompson, *Inorg. Chem.*, 2005, **44**, 1713-1727.
27. N. M. Shavaleev, F. Monti, R. D. Costa, R. Scopelliti, H. J. Bolink, E. Orti, G. Accorsi, N. Armaroli, E. Baranoff, M. Gratzel and M. K. Nazeeruddin, *Inorg. Chem.*, 2012, **51**, 2263-2271.
28. N. M. Shavaleev, F. Monti, R. Scopelliti, N. Armaroli, M. Gratzel and M. K. Nazeeruddin, *Organometallics*, 2012, **31**, 6288-6296.
29. N. M. Shavaleev, F. Monti, R. Scopelliti, A. Baschieri, L. Sambri, N. Armaroli, M. Gratzel and M. K. Nazeeruddin, *Organometallics*, 2013, **32**, 460-467.
30. D. Di Censo, S. Fantacci, F. De Angelis, C. Klein, N. Evans, K. Kalyanasundaram, H. J. Bolink, M. Gratzel and M. K. Nazeeruddin, *Inorg. Chem.*, 2008, **47**, 980-989.
31. H. Na, P. N. Lai, L. M. Cañada and T. S. Teets, *Organometallics*, 2018, **37**, 3269-3277.
32. L. Wallace and D. P. Rillema, *Inorganic Chemistry*, 1993, **32**, 3836-3843.
33. D. S. Tyson, K. B. Henbest, J. Bialecki and F. N. Castellano, *J. Phys. Chem. A.*, 2001, **105**, 8154-8161.

34. D. S. Tyson, C. R. Luman, X. Zhou and F. N. Castellano, *Inorg. Chem.*, 2001, **40**, 4063-4071.
35. J. E. Yarnell, J. C. Deaton, C. E. McCusker and F. N. Castellano, *Inorg. Chem.*, 2011, **50**, 7820-7830.
36. J. E. Yarnell, C. E. McCusker, A. J. Leeds, J. M. Breaux and F. N. Castellano, *Eur. J. Inorg. Chem.*, 2016, 1808-1818.
37. E. A. Medlycott, G. S. Hanan, F. Loiseau and S. Campagna, *Chemistry – A European Journal*, 2007, **13**, 2837-2846.
38. L. Wallace, D. C. Jackman, D. P. Rillema and J. W. Merkert, *Inorganic Chemistry*, 1995, **34**, 5210-5214.
39. J. M. Favale, E. O. Danilov, J. E. Yarnell and F. N. Castellano, *Inorg. Chem.*, 2019, **58**, 8750-8762.
40. C. E. McCusker, A. Chakraborty and F. N. Castellano, *J. Phys. Chem. A.*, 2014, **118**, 10391-10399.
41. K. Suzuki, A. Kobayashi, S. Kaneko, K. Takehira, T. Yoshihara, H. Ishida, Y. Shiina, S. Oishi and S. Tobita, *Phys. Chem. Chem. Phys.*, 2009, **11**, 9850-9860.
42. S. Garakyaraghi, E. O. Danilov, C. E. McCusker and F. N. Castellano, *J. Phys. Chem. A.*, 2015, **119**, 3181-3193.
43. M. J. Frisch, G. W. Trucks, H. B. Schlegel, G. E. Scuseria, M. A. Robb, J. R. Cheeseman, G. Scalmani, V. Barone, B. Mennucci, G. A. Petersson, H. Nakatsuji, M. Caricato, X. Li, H. P. Hratchian, A. F. Izmaylov, J. Bloino, G. Zheng, J. L. Sonnenberg, M. Hada, M. Ehara, K. Toyota, R. Fukuda, J. Hasegawa, M. Ishida, T. Nakajima, Y. Honda, O. Kitao, H. Nakai, T. Vreven, J. A. Montgomery, Jr.; , J. E. Peralta, F. Ogliaro, M. Bearpark, J. J. B. Heyd, E.; , K. N. Kudin, V. N. Staroverov, R. Kobayashi, J. Normand, K. Raghavachari, A. Rendell, J. C. Burant, S. S. Iyengar, J. Tomasi, M. Cossi, N. Rega, J. M. Millam, M. Klene, J. E. Knox, J. B. Cross, V. Bakken, C. Adamo, J. Jaramillo, R. Gomperts, R. E. Stratmann, O. Yazyev, A. J. Austin, R. Cammi, C. Pomelli, J. W. Ochterski, R. L. Martin, K. Morokuma, V. G. Zakrzewski, G. A. Voth, P. Salvador, J. J. Dannenberg, S. Dapprich, A. D. Daniels, Ö. Farkas, J. B. Foresman, J. V. Ortiz, J. Cioslowski and D. J. Fox *Gaussian 09 Rev. D.01*, Gaussian, Inc: Wallingford, CT, 2009.
44. Y. Zhao and D. G. Truhlar, *Theor. Chem. Acc.*, 2008, **120**, 215-241.
45. F. Weigend and R. Ahlrichs, *Phys. Chem. Chem. Phys.*, 2005, **7**, 3297-3305.
46. D. Andrae, U. Häußermann, M. Dolg, H. Stoll and H. Preuß, *Theor. Chim. Acta*, 1990, **77**, 123-141.
47. M. Cossi, G. Scalmani, N. Rega and V. Barone, *J. Chem. Phys.*, 2002, **117**, 43-54.
48. R. E. Stratmann, G. E. Scuseria and M. J. Frisch, *J. Chem. Phys.*, 1998, **109**, 8218-8224.
49. R. Bauernschmitt and R. Ahlrichs, *Chem. Phys. Lett.*, 1996, **256**, 454-464.
50. M. E. Casida, C. Jamorski, K. C. Casida and D. R. Salahub, *J. Chem. Phys.*, 1998, **108**, 4439-4449.
51. R. Dennington, T. Keith and J. Millam *Gaussview, Version 5*, Semichem Inc: Shawnee Mission, KS, 2009.
52. D. S. Tyson and F. N. Castellano, *J. Phys. Chem. A.*, 1999, **103**, 10955-10960.
53. D. S. Tyson, J. Bialecki and F. N. Castellano, *Chem. Commun.*, 2000, 2355-2356.
54. D. E. Polyansky, E. O. Danilov and F. N. Castellano, *Inorg. Chem.*, 2006, **45**, 2370-2372.

The degree of ancillary ligand conjugation determines Ir(III) polychromophoric photophysical properties via manipulation of the triplet excited state manifolds.

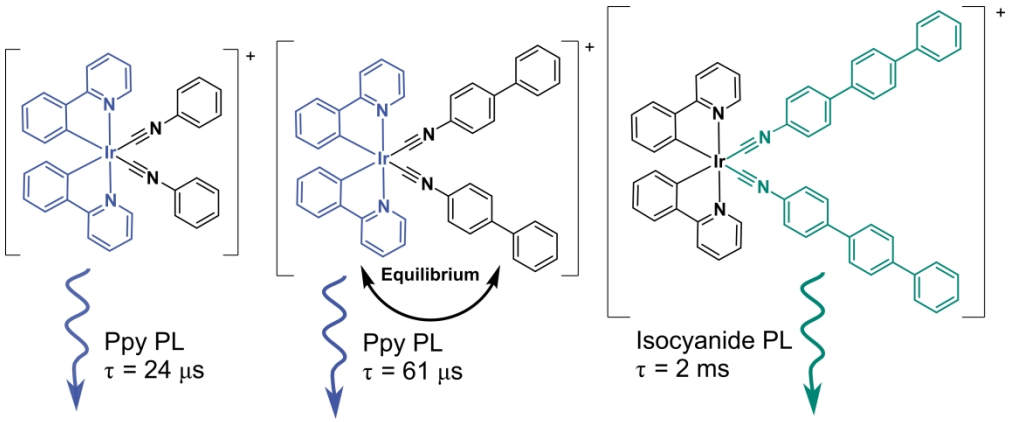
Ir
N
+
Equilibrium
Ppy PL
τ = 24 μs
Ppy PL
τ = 61 μs
Isocyanide PL
τ = 2 ms